



HAL
open science

High Field Superconducting Phases of Ultra Clean Single Crystal UTe₂

Dai Aoki, Ilya Sheikin, Nils Marquardt, Gerard Lapertot, Jacques Flouquet,
Georg Knebel

► **To cite this version:**

Dai Aoki, Ilya Sheikin, Nils Marquardt, Gerard Lapertot, Jacques Flouquet, et al.. High Field Superconducting Phases of Ultra Clean Single Crystal UTe₂. *Journal of the Physical Society of Japan*, 2024, 93 (12), 10.7566/JPSJ.93.123702 . hal-04830852

HAL Id: hal-04830852

<https://hal.science/hal-04830852v1>

Submitted on 11 Dec 2024

HAL is a multi-disciplinary open access archive for the deposit and dissemination of scientific research documents, whether they are published or not. The documents may come from teaching and research institutions in France or abroad, or from public or private research centers.

L'archive ouverte pluridisciplinaire **HAL**, est destinée au dépôt et à la diffusion de documents scientifiques de niveau recherche, publiés ou non, émanant des établissements d'enseignement et de recherche français ou étrangers, des laboratoires publics ou privés.



Distributed under a Creative Commons Attribution 4.0 International License

High Field Superconducting Phases of Ultra Clean Single Crystal UTe_2

Dai Aoki^{1*}, Ilya Sheikin², Nils Marquardt^{2,3}, Gerard Lapertot³, Jacques Flouquet^{1,3}, and Georg Knebel³,

¹*IMR, Tohoku University, Oarai, Ibaraki 311-1313, Japan*

²*LNCMI-EMFL, CNRS, UGA, 38042 Grenoble, France*

³*Univ. Grenoble Alpes, CEA, Grenoble INP, IRIG, PHELIQS, F-38000 Grenoble, France*

We report the magnetoresistance of high-quality single crystals of UTe_2 with $T_c = 2.1$ K in high magnetic fields up to 36 T, with the field direction between the b and c -axes. From the angular dependence of the upper critical field H_{c2} , we found that the field-reentrant superconducting phase near $H \parallel b$ -axis extends up to a field angle ($\theta \sim 24$ deg) from the b to c -axis, where another field-reentrant superconducting phase begins to appear above the metamagnetic transition field, H_m . Our results suggest that the field-reentrant superconductivity below H_m near the b -axis is closely related to the superconductivity above H_m when the field is tilted toward the c -axis. Superconductivity appears to be robust when the field direction is maintained perpendicular to the magnetization easy axis, implying that fluctuations boosting superconductivity may persist. At first glance, these findings resemble the field-reentrant (reinforced) superconductivity observed in ferromagnetic superconductors URhGe and UCoGe, where Ising-type ferromagnetic fluctuations play a crucial role. However, in UTe_2 , the fluctuations are more complex. The angular dependence of the upper critical field H_{c2} contrasts with that of the initial slope of H_{c2} near T_c , revealing the anisotropic field response of fluctuations. Thanks to the high-quality samples, quantum oscillations were detected for field directions close to the c -axis using magnetoresistance (Shubnikov-de Haas effect) and torque (de Haas-van Alphen effect) measurements. The angular dependence of frequencies is in good agreement with those observed previously using the field-modulation technique, confirming quasi-two dimensional Fermi surfaces.

UTe_2 attracts much attention because of unusual superconducting properties.¹⁻³ UTe_2 has a paramagnetic ground state with a heavy electronic state associated with the Sommerfeld coefficient $\gamma \sim 120$ mJ K⁻² mol⁻¹. Superconductivity occurs at $T_c \sim 1.6$ – 2.1 K. It had been suggested that UTe_2 would be an end member of ferromagnetic superconductors, such as UGe₂,⁴ URhGe⁵ and UCoGe.⁶ However, no ferromagnetic fluctuations are experimentally established in UTe_2 . Alternatively, antiferromagnetic fluctuations with an incommensurate wave-vector were detected in inelastic neutron scattering experiments.^{7,8} Furthermore, an antiferromagnetic order appears above the critical pressure, $P_c \sim 1.5$ GPa.^{9,10} Thus, the magnetic properties and the mechanism of superconductivity for UTe_2 are more complicated, compared to those for ferromagnetic superconductors.

The highlight of UTe_2 is that superconductivity is quite robust against magnetic field, and the superconducting upper critical field, H_{c2} , highly exceeds the Pauli limit in all field directions. Moreover, when the field is applied along the hard-magnetization b -axis, field-reentrant superconductivity is realized, and it is abruptly suppressed due to the first-order metamagnetic transition at $H_m \sim 35$ T.^{11,12} This huge H_{c2} associated with the field-reentrant behavior is consistent with a scenario for spin-triplet superconductivity. Another strong support for the spin-triplet state is the emergence of multiple superconducting phases under pressure^{13,14} and at high fields,¹⁵ which might be a consequence of spin and orbital

degrees of freedom in spin-triplet superconductivity.

The angular dependence of H_{c2} is also remarkable. By rotating the field direction from b to c -axis, maintaining the field perpendicular to the easy-magnetization a -axis, H_m increases with the field angle θ , following the $1/\cos\theta$ dependence. Reentrant superconductivity disappears at $\theta \sim 10$ deg, but reappears above H_m at $\theta \sim 24$ – 45 deg.^{12,16} These results were obtained using UTe_2 single crystals with $T_c \sim 1.6$ K.

Recently, the angular dependence of H_{c2} and H_m using a high quality single crystal with $T_c = 2.1$ K at low temperatures down to ~ 0.4 K was reported.¹⁷ The field-reentrant superconducting phase near $H \parallel b$ -axis is expanded down to $\theta \sim 21$ deg.

It is important to study the angular dependence of H_{c2} and H_m more precisely at lower temperatures using a high quality sample with $T_c = 2.1$ K. In this study, we performed magnetoresistance measurements in high quality samples by rotating the field angle, θ , from b to c -axis. We found that the field-reentrant superconducting phase expands up to $\theta \sim 24$ deg $\sim \arctan(b/c)$, where b and c are lattice constants, corresponding to the [011] direction in the reciprocal space, which we describe [011]*. Further increasing θ , the field-reentrant superconductivity is extended above H_m . Our results indicate that the field-reentrant superconductivity below H_m is highly related to that above H_m for $\theta \gtrsim 24$ deg. The angular dependence of H_{c2} is compared to that of the initial slope of H_{c2} near T_c , revealing a clear contrast between them. Furthermore the quantum oscillations are detected near $H \parallel c$ -axis as Shubnikov-de Haas (SdH) and de Haas-van Alphen (dHvA)

*E-mail: aoki@imr.tohoku.ac.jp

effects, through magnetoresistance and torque measurements, respectively. The angular dependence of the frequencies is in good agreement with those obtained by the field modulation technique.^{18, 19)}

High quality single crystals were grown using the molten salt flux (MSF) and the molten salt flux liquid transport (MSFLT) methods as described in Refs. 20, 21. Many as-grown crystals show the (001) as well as (011) plane, which can be easily cleaved, indicating that the [011]* direction is a unique direction. Sharp Laue spots in the X-ray diffraction and a sharp specific heat jump at $T_c = 2.1$ K with the small residual γ -value ($\gamma_0/\gamma_N \sim 0.03$) indicate the high quality of our samples. The residual resistivity is $\rho_0 \sim 0.63 \mu\Omega \cdot \text{cm}$ and the residual resistivity ratio is $\text{RRR} \sim 500$, indicating also the exceptional quality. The magnetoresistance was measured using the four-probe AC method at high fields up to 36 T using a resistive magnet and at temperatures down to 55 mK in a top-loading dilution fridge equipped with a swedish rotator. The low-field magnetoresistance was supplementally measured at fields up to 13 and 15 T in dilution fridges. The electrical current was applied along the a -axis and the samples were rotated from $H \parallel b$ to c -axis and from $H \parallel b$ to a -axis. The torque measurements for the dHvA effect were performed close to $H \parallel c$ -axis, using a cantilever at high fields up to 36 T and at low temperatures down to 0.06 K. For the initial slope of H_{c2} , AC calorimetry measurements were performed near T_c using a AuFe-Au thermocouple for the field directions between a , b and c -axes with a rotator.

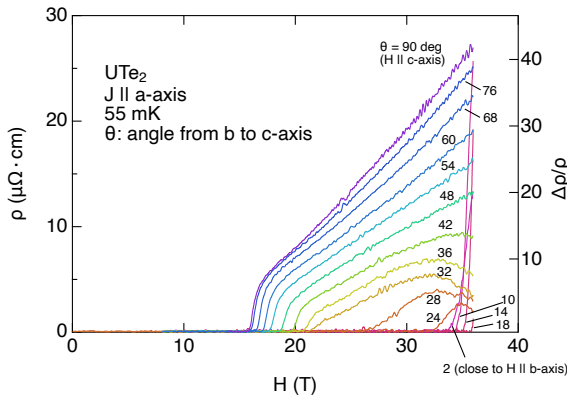


Fig. 1. (Color online) Magnetoresistance at 55 mK at different field angles tilted from $H \parallel b$ to c -axis in UTe_2 . The electrical current is applied along a -axis. The right axis indicates $\Delta\rho/\rho \equiv [\rho(H) - \rho(0)]/\rho(0)$, where $\rho(0)$ is the resistivity at zero field expected in the normal state.

Figure 1 shows the magnetoresistance at 55 mK at different field directions from b to c -axis with the current along a -axis, maintaining the transverse configuration. For the field direction close to b -axis ($\theta \sim 2$ deg), superconductivity survives up to $H_{c2} = 34$ T and the resistivity starts to increase because of the recovery to the normal state associated with the metamag-

netic transition. Note that the normal state is not fully recovered at our highest field, 36 T. Increasing θ slightly, the onset field of magnetoresistance also slightly increases due to the increase of H_m , which follows the $1/\cos\theta$ -dependence. But at $\theta = 24$ deg, the magnetoresistance shows the finite value already at 32 T and then decreases again above 34 T, indicating the sign of reappearance of superconductivity at high fields. The decrease of magnetoresistance at high fields is observed up to $\theta = 42$ deg, indicating the field-reentrant superconductivity is likely to appear at high fields above 36 T at least for $\theta \sim 24$ –42 deg. Further increasing θ , H_{c2} decreases and the resistivity in the normal state at 36 T increases. For $H \parallel c$ -axis, the value of H_{c2} defined by zero resistivity is 15.9 T. Note that SdH oscillations are already visible without subtracting the background for $H \parallel c$ -axis above 20 T, and the magnetoresistance is large, ($\Delta\rho/\rho > 40$), confirming the high quality of our sample. The large (small) magnetoresistance along c (b)-axis for the current along a -axis indicates the existence of open orbits along c -axis in this compensated metal, which is consistent with the cylindrical Fermi surfaces along c -axis detected by previous dHvA experiments.^{18, 19, 22)}

Figure 2(a) shows the complete angular dependence of H_{c2} and the metamagnetic transition field H_m . The present results obtained by the magnetoresistance (closed circles and triangles) are combined with our results of AC susceptibility (closed squares) reported previously¹⁸⁾ and the results of magnetoresistance, PDO and torque measurements around 0.4 K (open symbols).^{12, 16, 17)} For the field direction close to b -axis, H_{c2} is limited by H_m , which increases with the field angle, θ , following the $1/\cos\theta$ -dependence. At $\theta \sim 24$ deg, H_{c2} is remarkably dropped, while H_m continuously increases. Interestingly, field-reentrant superconductivity starts to appear above ~ 24 deg, and persists up to ~ 50 deg^{12, 16, 17)} As shown in Fig. 1, the sign of field-reentrant superconductivity above H_m is observed at high fields, and the linear extrapolation of the decrease of magnetoresistance gives the starting field of reentrant superconductivity, which agrees well with the previously reported values.^{12, 16)}

The angular dependence shown in Fig. 2(a) differs somewhat from that observed in the lower quality sample ($T_c \sim 1.6$ K). In the samples with $T_c \sim 1.6$ K, field-reentrant superconductivity near b -axis is terminated at $\theta \sim 10$ deg,¹¹⁾ and field reentrant superconductivity above H_m for $\theta \sim 24$ –40 deg is isolated. However, in high quality samples with $T_c \sim 2.1$ K, both field-reentrant superconductivities are almost connected at $\theta \sim 24$ deg at $H_m \sim 40$ T. Here we choose a rather strict definition for superconductivity, which is given by the zero resistivity. Field-reentrant superconductivity below H_m may further extend up to ~ 40 deg if we take a loose definition.

The angular dependences of H_{c2} for $H \parallel b \rightarrow a$ -axis and $H \parallel c \rightarrow a$ -axis are also unusual. For instance, H_{c2} between c and a -axes shows a broad minimum at $\theta \sim 45$ –60 deg with a sharp maximum at $H \parallel a$ -axis. Of course, this cannot be explained by a conventional effective mass model, implying the anisotropic field-response of fluctuations or a multicomponent of order parameters.²³⁾

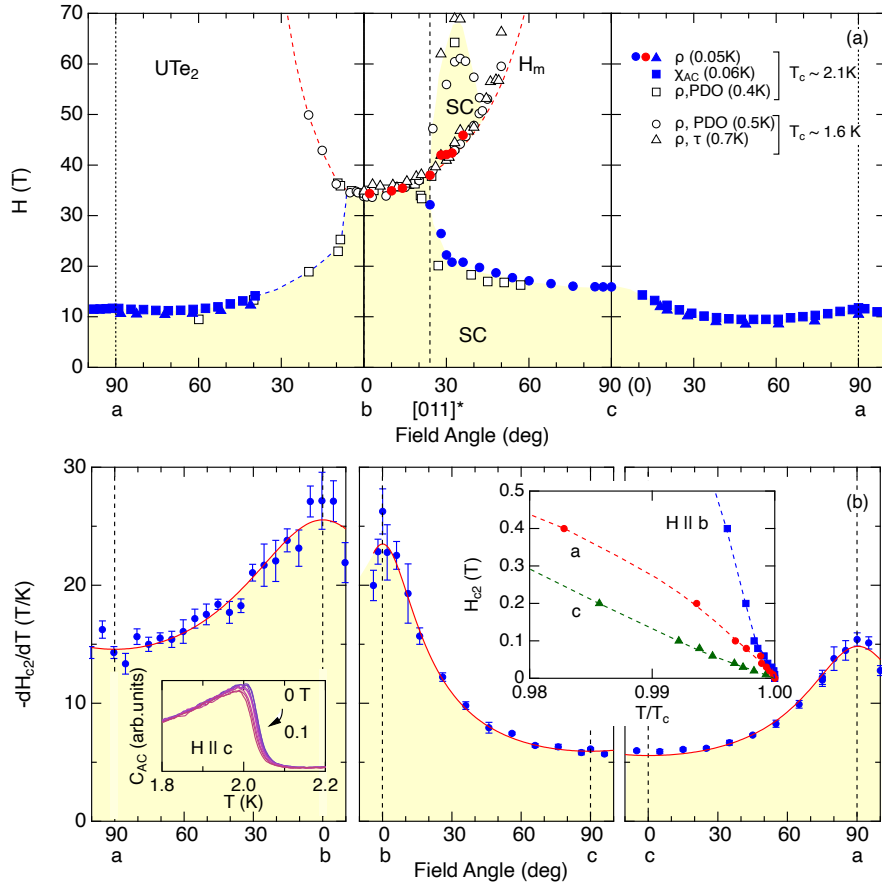


Fig. 2. (Color online) (a) Angular dependence of H_{c2} and the metamagnetic transition field H_m in UTe_2 with high quality ($T_c \sim 2.1$ K). Closed circles and triangles are the results of magnetoresistance using a resistive and superconducting magnet, respectively. Closed squares are the results of AC susceptibility.¹⁸⁾ Open squares are the results of magnetoresistance and TDO at ~ 0.4 K.¹⁷⁾ High field results above 35 T in lower quality samples ($T_c \sim 1.6$ K) are also plotted. Open circles are the results of magnetoresistance and TDO at ~ 0.5 K.¹²⁾ Open triangles are the results of magnetoresistance and torque at ~ 0.7 K.¹⁶⁾ (b) Angular dependence of the initial slope of H_{c2} near T_c determined by the AC calorimetry measurements in the field range between 0 to 0.1 T in UTe_2 . The error bars are from the linear fitting. Red lines are the results of the effective mass model. The right-top inset shows the H_{c2} curves near T_c for $H \parallel a, b$ and c -axis. Temperature is scaled by T_c . The left-bottom inset shows the AC calorimetry at 0, 0.01, 0.02, 0.03, 0.04, 0.06, 0.08 and 0.1 T for $H \parallel c$ -axis.

In order to clarify the H - T phase diagram at the border of two reentrant superconducting phases below/above H_m , we measured the magnetoresistance at $\theta \sim 24$ deg ($H \parallel [011]^*$) at different temperatures, as shown in Fig. 3(a). At the lowest temperature, 0.058 K, magnetoresistance shows a finite values above 32 T, but it decreases again above 35 T, revealing the field-reentrant superconducting behavior. Extrapolating the decrease of magnetoresistance linearly, the magnetoresistance is expected to be zero at about 38 T, which is close to the metamagnetic transition field, $H_m \sim 38$ T for $\theta \sim 24$ deg. The decrease of magnetoresistance at high fields is observed up to 0.6 K, suggesting reentrant superconductivity survives at least up to 0.6 K.

Figure 3(b) shows the H - T phase diagram for $H \parallel [011]^*$. The critical field of superconductivity here is defined by zero resistivity. The H_{c2} curve shows the slight convex curvature at low fields below 18 T, but the slope abruptly increases above

18 T. Finally superconductivity is suppressed at 32 T. Further increasing fields, superconductivity reappears above ~ 38 T, which almost coincides with metamagnetic transition field, H_m . The reentrant superconducting phase above H_m will be extended to the higher temperature at $H \gtrsim H_m$, as shown in Fig. 3(a), which is expected from the results obtained previously in lower quality samples. Here we take a strict definition for superconductivity as zero resistivity. If we define the superconducting phase by the onset of resistivity drop, superconducting phases below and above H_m will be merged.

Note that the $[011]^*$ direction could be a specific direction for superconductivity. Although we do not yet have a clear explanation, it is worth mentioning that the $[011]^*$ direction corresponds to a cleaving plane where charge density waves (CDW) and pair density waves (PDW) associated with superconductivity have been detected on the surface through STM experiments.^{24,25)} Furthermore, it has been proposed that the

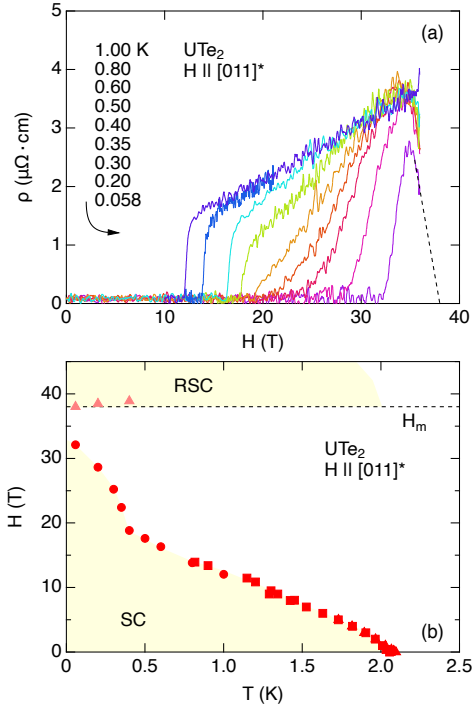


Fig. 3. (Color online) (a) Magnetoresistance at different temperatures for the field along the [011]^{*} direction (field angle: $\theta \sim 24$ deg from b to c -axis) in UTe₂. (b) H - T phase diagram for the field along the [011]^{*} direction. Closed circles and closed squares are the results of magnetoresistance defined by zero resistivity in the resistive and superconducting magnet, respectively. Closed triangles are the estimated critical fields for reentrant superconductivity from the linear extrapolation of magnetoresistance, which is shown for instance, as a dashed line at 0.058 K in panel (a).

[011]^{*} direction may switch to the c -axis direction in the tetragonal phase under pressures above 4 GPa after the structural phase transition.²⁶⁾

It is interesting to compare the angular dependence of H_{c2} with that of the initial slope of H_{c2} near T_c . Figure 2(b) shows the angular dependence of the initial slope of H_{c2} near T_c , determined by the AC calorimetry measurements, which were done at different constant fields at different field angles. The left-bottom inset of Fig. 2(b) shows an example for $H \parallel c$ -axis at low fields up to 0.1 T. The initial slopes of H_{c2} , that is, $-dH_{c2}/dT$, were obtained by the linear fitting of H_{c2} up to 0.1 T at different field angles. The initial slopes for $H \parallel a$, b , and c -axis are 15, ~ 25 , and 5.9 T/K, respectively, showing a strong anisotropy. For $H \parallel b$ -axis, the initial slope is very large, and the slope changes rapidly with field, as shown in the right-top inset of Fig. 2. The initial slope for $H \parallel a$ -axis is also large with a convex curvature. On the other hand, the initial slope for $H \parallel c$ -axis is small, and H_{c2} increases linearly. The values of initial slopes are slightly different from those reported previously,¹⁵⁾ probably due to the linear range of H_{c2} and the definition.

The small initial slope for $H \parallel c$ -axis compared to those for

$H \parallel a$ and b -axis is consistent with the quasi-2D Fermi surfaces detected by the dHvA experiments. More precisely, the angular dependence of the initial slope should be described by the so-called effective mass model, which can be simply described by $H_{c2}(\theta) = H_{c2}(90^\circ)/(\sin^2 \theta + m_c^*/m_a^* \cos^2 \theta)^{1/2}$, assuming an ellipsoidal Fermi surface with anisotropic effective mass as an average between c and a -axis. Here one can replace H_{c2} as $-dH_{c2}/dT$. The same model can be applied to the anisotropy between c and b -axes by replacing m_a with m_b . The mass anisotropy obtained by fitting with an effective mass model is 7.1 for m_a/m_c and 16 for m_b/m_c . The smaller mass anisotropy for m_a/m_c is consistent with the anisotropy of magnetic susceptibilities at low temperatures, where the susceptibility for a -axis is the largest among the principal field directions.

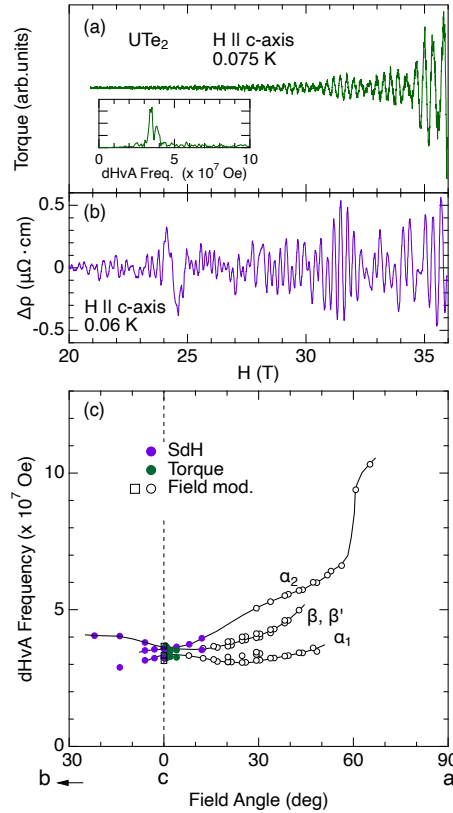


Fig. 4. (Color online) (a) dHvA oscillations and the FFT spectrum (inset) detected by torque measurements and (b) SdH oscillations for $H \parallel c$ -axis in UTe₂ after subtracting the background signals. (c) Angular dependence of the dHvA (SdH) frequencies. Solid circles are obtained from the torque and SdH experiments. Open circles and squares are the results of our previous dHvA experiments by field-modulation technique.^{18,19)}

Finally we show the quantum oscillations near $H \parallel c$ -axis detected by magnetoresistance (SdH) and torque (dHvA) measurements. Figures 4(a) and 4(b) show dHvA and SdH oscillations, respectively, for $H \parallel c$ -axis, after subtracting

the background signals. Thanks to high quality of the samples, clear quantum oscillations are detected above 20 T for SdH effect and above 25 T for dHvA effect. The FFT analysis yields three fundamental frequencies ranging from 3.3 to 3.8 kT, which correspond to branches α_1 , β and α_2 , respectively. The cyclotron effective masses are 33–34 m_0 , which are also in good agreement with the previously obtained values.^{18,19)}

The angular dependence of dHvA (SdH) frequencies are shown in Fig. 4(c), together with the dHvA frequencies obtained by the previous experiments through the field-modulation technique.^{18,19)} The present results show a good agreement with the previous results, and further extend the angular dependence near $H \parallel c$ -axis for the directions from c to a -axis and from c to b -axis. Note that we did not detect any low frequencies other than these fundamental frequencies in difference to Ref. 27

In summary, we performed high field magnetoresistance up to 36 T for the field direction from b to c -axis using the high-quality single crystals of UTe₂ with $T_c = 2.1$ K. The overall angular dependence of H_{c2} shows higher values corresponding to higher T_c , compared to those obtained in lower-quality samples. For the field directions close to the b -axis, superconductivity is cut off by the first-order metamagnetic transition at H_m , insensitive to the sample quality. Remarkably, the field-reentrant superconducting phase near $H \parallel b$ -axis extends to the field angle $\theta \sim 24$ deg, where reentrant superconductivity starts to appear above H_m . Superconductivity is quite robust when the field direction is maintained perpendicular to the easy magnetization a -axis. These properties appear to be similar to those observed in ferromagnetic superconductors, URhGe²⁸⁾ and UCoGe,²⁹⁾ in which ferromagnetic fluctuations are not suppressed or even induced at high fields.^{30,31)} However, in UTe₂, magnetic fluctuations or other fluctuations are likely to be more complicated, in addition, associated with the first-order metamagnetic transition, which could make a drastic change of Fermi surfaces. Another key issue is the interplay between ferromagnetic and antiferromagnetic fluctuations, which may have quite different field-response. The angular dependence of the initial slope of H_{c2} reflects the quasi-2D Fermi surfaces. The quantum oscillations detected by SdH and torque dHvA experiments provided several additional data points near $H \parallel c$ -axis in the angular dependence of the oscillatory frequencies, which are in good agreement with the previous results measured at lower fields.

Acknowledgements

We thank J. P. Brison, D. Braithwaite, T. Helm, M. Kimata, Y. Homma, D. X. Li, A. Nakamura, Y. Shimizu and A. Miyake for fruitful discussion and technical support. This work was supported by KAKENHI (JP19H00646, JP20K20889, JP20H00130, JP20KK0061, JP22H04933, JP24H01641), the French ANR projects, SCATE (ANR-22-CE30-0040), FRESCO (ANR-20-CE30-0020), FETTOM (ANR-19-CE30-0037) We acknowledge support from LNCMI-CNRS, member of the European

Magnetic Field Laboratory (EMFL), and the Laboratoire d'excellence LANEF (ANR-10-LABX-0051).

- 1) S. Ran, C. Eckberg, Q.-P. Ding, Y. Furukawa, T. Metz, S. R. Saha, I.-L. Liu, M. Zic, H. Kim, J. Paglione, and N. P. Butch: *Science* **365**, 684 (2019).
- 2) D. Aoki, A. Nakamura, F. Honda, D. Li, Y. Homma, Y. Shimizu, Y. J. Sato, G. Knebel, J.-P. Brison, A. Pourret, D. Braithwaite, G. Lapertot, Q. Niu, M. Vališka, H. Harima, and J. Flouquet: *J. Phys. Soc. Jpn.* **88**, 043702 (2019).
- 3) D. Aoki, J. P. Brison, J. Flouquet, K. Ishida, G. Knebel, Y. Tokunaga, and Y. Yanase: *J. Phys.: Condens. Matter* **34**, 243002 (2022).
- 4) S. S. Saxena, P. Agarwal, K. Ahilan, F. M. Grosche, R. K. W. Haselwimmer, M. J. Steiner, E. Pugh, I. R. Walker, S. R. Julian, P. Monthoux, G. G. Lonzarich, A. Huxley, I. Sheikin, D. Braithwaite, and J. Flouquet: *Nature* **406**, 587 (2000).
- 5) D. Aoki, A. Huxley, E. Ressouche, D. Braithwaite, J. Flouquet, J.-P. Brison, E. Lhotel, and C. Paulsen: *Nature* **413**, 613 (2001).
- 6) N. T. Huy, A. Gasparini, D. E. de Nijs, Y. Huang, J. C. P. Klaasse, T. Gortenmulder, A. de Visser, A. Hamann, T. Görlach, and H. v. Löhneysen: *Phys. Rev. Lett.* **99**, 067006 (2007).
- 7) C. Duan, K. Sasmal, M. B. Maple, A. Podlesnyak, J.-X. Zhu, Q. Si, and P. Dai: *Phys. Rev. Lett.* **125**, 237003 (2020).
- 8) W. Knafo, M. Nardone, M. Vališka, A. Zitouni, G. Lapertot, D. Aoki, G. Knebel, and D. Braithwaite: *Commun. Phys.* **4**, 40 (2021).
- 9) W. Knafo, T. Thebault, P. Manuel, D. D. Khalyavin, F. Orlandi, E. Ressouche, K. Beauvois, G. Lapertot, K. Kaneko, D. Aoki, D. Braithwaite, G. Knebel, and S. Raymond: arXiv:2311.05455.
- 10) D. Li, A. Nakamura, F. Honda, Y. J. Sato, Y. Homma, Y. Shimizu, J. Ishizuka, Y. Yanase, G. Knebel, J. Flouquet, and D. Aoki: *J. Phys. Soc. Jpn.* **90**, 073703 (2021).
- 11) G. Knebel, W. Knafo, A. Pourret, Q. Niu, M. Vališka, D. Braithwaite, G. Lapertot, J.-P. Brison, S. Mishra, I. Sheikin, G. Seyfarth, D. Aoki, and J. Flouquet: *J. Phys. Soc. Jpn.* **88**, 063707 (2019).
- 12) S. Ran, I.-L. Liu, Y. S. Eo, D. J. Campbell, P. Neves, W. T. Fuhrman, S. R. Saha, C. Eckberg, H. Kim, J. Paglione, D. Graf, J. Singleton, and N. P. Butch: *Nature Phys.* **15**, 1250 (2019).
- 13) D. Braithwaite, M. Vališka, G. Knebel, G. Lapertot, J. P. Brison, A. Pourret, M. E. Zhitomirsky, J. Flouquet, F. Honda, and D. Aoki: *Commun. Phys.* **2**, 147 (2019).
- 14) D. Aoki, F. Honda, G. Knebel, D. Braithwaite, A. Nakamura, D. Li, Y. Homma, Y. Shimizu, Y. J. Sato, J.-P. Brison, and J. Flouquet: *J. Phys. Soc. Jpn.* **89**, 053705 (2020).
- 15) A. Rosuel, C. Marcenat, G. Knebel, T. Klein, A. Pourret, N. Marquardt, Q. Niu, S. Rousseau, A. Demuer, G. Seyfarth, G. Lapertot, D. Aoki, D. Braithwaite, J. Flouquet, and J. P. Brison: *Phys. Rev. X* **13**, 011022 (2023).
- 16) T. Helm, M. Kimata, K. Sudo, A. Miyata, J. Stirnat, T. Förster, J. Hornung, M. König, I. Sheikin, A. Pourret, G. Lapertot, D. Aoki, G. Knebel, J. Wosnitza, and J.-P. Brison: *Nat. Commun.* **15**, 37 (2024).
- 17) Z. Wu, T. I. Weinberger, J. Chen, A. Cabala, D. V. Chichinadze, D. Shaffer, J. Pospíšil, J. Prokleška, T. Haidamak, G. Bastien, V. Sechovský, A. J. Hickey, M. J. Mancera-Ugarte, S. Benjamin, D. E. Graf, Y. Skourski, G. G. Lonzarich, M. Vališka, F. M. Grosche, and A. G. Eaton: *PNAS* **121**, e2403067121 (2024).
- 18) D. Aoki, H. Sakai, P. Opletal, Y. Tokiwa, J. Ishizuka, Y. Yanase, H. Harima, A. Nakamura, D. Li, Y. Homma, Y. Shimizu, G. Knebel, J. Flouquet, and Y. Haga: *J. Phys. Soc. Jpn.* **91**, 083704 (2022).
- 19) D. Aoki, I. Sheikin, A. McCollam, J. Ishizuka, Y. Yanase, G. Lapertot, J. Flouquet, and G. Knebel: *J. Phys. Soc. Jpn.* **92**, 065002 (2023).
- 20) H. Sakai, P. Opletal, Y. Tokiwa, E. Yamamoto, Y. Tokunaga, S. Kambe, and Y. Haga: *Phys. Rev. Mater.* **6**, 073401 (2022).
- 21) D. Aoki: *J. Phys. Soc. Jpn.* **93**, 043703 (2024).
- 22) A. G. Eaton, T. I. Weinberger, N. J. M. Popiel, Z. Wu, A. J. Hickey,

- A. Cabala, J. Pospíšil, J. Prokleška, T. Haidamak, G. Bastien, P. Opletal, H. Sakai, Y. Haga, R. Nowell, S. M. Benjamin, V. Sechovský, G. G. Lonzarich, F. M. Grosche, and M. Vališka: *Nat. Commun.* **15**, 223 (2024).
- 23) M. E. Zhitomirskii: *Sov. Phys. JETP* **70**, 760 (1990).
- 24) Q. Gu, J. P. Carroll, S. Wang, S. Ran, C. Broyles, H. Siddiquee, N. P. Butch, S. R. Saha, J. Paglione, J. S. Davis, , and X. Liu: *Nature* **618**, 921 (2023).
- 25) A. Aishwarya, J. May-Mann, A. Raghavan, L. Nie, M. Romanelli, S. Ran, S. R. Saha, J. Paglione, N. P. Butch, E. Fradkin, and V. Madhavan: *Nature* **618**, 928 (2023).
- 26) F. Honda, S. Kobayashi, N. Kawamura, S. I. Kawaguchi, T. Koizumi, Y. J. Sato, Y. Homma, N. Ishimatsu, J. Gouchi, Y. Uwatoko, H. Harima, J. Flouquet, and D. Aoki: *J. Phys. Soc. Jpn.* **92**, 044702 (2023).
- 27) C. Broyles, Z. Rehfuss, H. Siddiquee, K. Zheng, Y. Le, M. Nikolo, D. Graf, J. Singleton, and S. Ran: *Phys. Rev. Lett.* **131**, 036501 (2023).
- 28) F. Lévy, I. Sheikin, and A. Huxley: *Nature Physics* **3**, 460 (2007).
- 29) D. Aoki, T. D. Matsuda, V. Taufour, E. Hassinger, G. Knebel, and J. Flouquet: *J. Phys. Soc. Jpn.* **78**, 113709 (2009).
- 30) Y. Tokunaga, D. Aoki, H. Mayaffre, S. Krämer, M.-H. Julien, C. Berthier, M. Horvatić, H. Sakai, S. Kambe, and S. Araki: *Phys. Rev. Lett.* **114**, 216401 (2015).
- 31) T. Hattori, Y. Ihara, Y. Nakai, K. Ishida, Y. Tada, S. Fujimoto, N. Kawakami, E. Osaki, K. Deguchi, N. K. Sato, and I. Satoh: *Phys. Rev. Lett.* **108**, 066403 (2012).